

Abstract

This study seeks to help better understand aerosol-cloud interactions by examining statistical relationships between aerosol properties and nearby low-altitude cloudiness using satellite data. The analysis of a global dataset of MODIS (Moderate Resolution Imaging Spectroradiometer) observations reveals that the positive correlation between cloudiness and aerosol optical depth (AOD) reported in earlier studies is strong throughout the globe and during both winter and summer. Typically, AOD is 30-50% higher on cloudier-than-average days than on less cloudy days. A combination of satellite observations and MERRA-2 global reanalysis data reveals that the correlation between cloud cover and AOD is strong for all aerosol types considered: sulfate, dust, carbon, and sea salt.

The observations also indicate that in the presence of nearby clouds, aerosol size distributions tend to shift toward smaller particles over large regions of the Earth. This is consistent with a greater cloud-related increase in the AOD of fine mode than of coarse mode particles. The greater increase in fine mode AOD implies that the cloudiness-AOD correlation does not come predominantly from cloud detection uncertainties. Additionally, the results show that aerosol particle size increases near clouds even in regions where it decreases with increasing cloudiness. This suggests that the decrease with cloudiness comes mainly from changes in large-scale environment, rather than from clouds increasing the number or the size of fine mode aerosols. Finally, combining different aerosol retrieval algorithms demonstrated that quality assessment flags based on local variability can help identifying when the observed aerosol populations are affected by surrounding clouds.

1 Introduction

Clouds, aerosols, and their interactions are among the largest sources of uncertainty in estimating human impacts on climate. As stated in the Intergovernmental Panel on Climate Change 5th Assessment Report (IPCC AR5, 2013) Chapter 7, “*Clouds and aerosols continue to contribute the largest uncertainty to estimates and interpretations of the Earth’s changing energy budget ... the quantification ... of aerosol–cloud interactions continues to be a challenge.*”

Satellite observations have helped improve our understanding of aerosol-cloud interactions by providing observations on the relationships between aerosol and cloud properties. For example, analyzing a 4-year long global dataset of satellite observations, Loeb and Manalo-Smith (2005) found a positive correlation between cloud fraction (CF) and aerosol optical depth (AOD). Figure 1 shows that they found this relationship to be strong when using either NOAA or NASA satellite products. Other satellite studies also found positive correlations between CF and AOD [Ignatov *et al.*, 2005; Kaufman *et al.*, 2005; Zhang *et al.*, 2005; Chand *et al.*, 2012], or found that AOD increases in the vicinity of clouds [Loeb and Schuster, 2008; Tackett and Di Girolamo, 2009; Twohy *et al.*, 2009; Várnai *et al.*, 2013; Várnai and Marshak, 2014]. Similar tendencies were observed using ground-based and airborne measurements [Koren *et al.*, 2007; Su *et al.*, 2008; Ten Hoeve and Augustine, 2016] and also in modeling studies [Quaas *et al.*, 2010; Grandey *et al.*, 2013]. These studies identified several factors that likely contribute to the observed behaviors. For example, aerosol particles may swell in the humid air surrounding clouds [e.g., Twohy *et al.*, 2009; Jeong and Li, 2010], or clouds may foster the generation of new or larger aerosol particles through chemical reactions or microphysical cloud processing [Kerckweg *et al.*, 2003; Ervens *et al.*, 2011, Eck *et al.*, 2012]. On the other hand, higher aerosol contents may prolong the lifetime of clouds and thus increase cloud coverage in an area [e.g., Albrecht, 1989]. In some cases, remote sensing issues such as uncertainties in aerosol-cloud discrimination [Zhang *et al.*, 2005] or the 3D radiative process of clouds scattering sunlight into nearby clear areas may also contribute [Marshak *et al.*, 2008; Koren *et al.*, 2009; Wen *et al.*, 2008; Várnai and Marshak, 2009]. Complementing the papers that focused on individual processes, other studies examined the relative importance of several factors in shaping the observed overall behaviors. For example, Jeong and Li [2010] provided insights on the way cloud contamination, aerosol swelling, and the formation of new aerosol particles affect the relationship between CF and AOD.

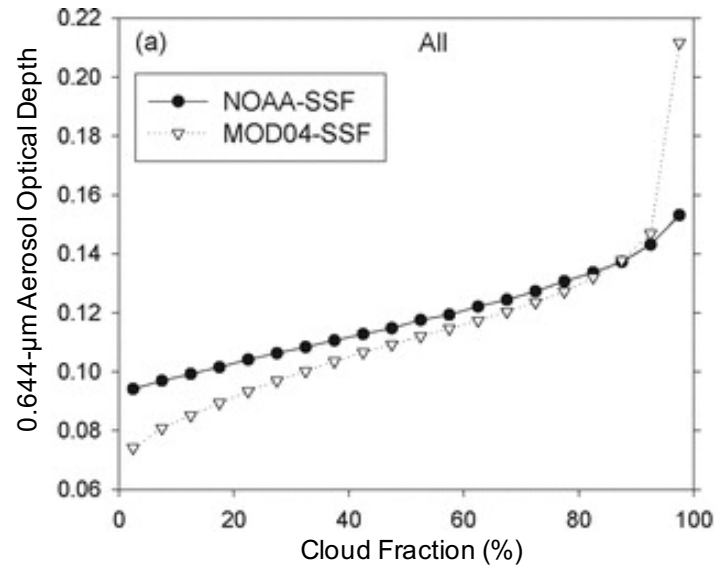


Figure 1. Relationship over global oceans between regional cloud fraction and mean aerosol optical depth. This figure is a reproduction of Fig. 6a in *Loeb and Manalo-Smith [2005]*. Both curves are based on data from the Terra satellite’s MODIS instrument, but they were obtained using two different cloud masking algorithms: a NOAA algorithm and the NASA algorithm used for producing the operational aerosol product.

Despite the numerous insights provided by such studies, some important questions still remain. This paper examines two such questions: (i) How does the CF-AOD relationship vary with location and aerosol type? (ii) What is the relationship between cloudiness and aerosol particle size distributions? (We note that, in addition to being important for radiative transfer and other physical and chemical processes, particle size is also a key factor in the aerosol index that is becoming more commonly used in aerosol-cloud studies (e.g., Chen et al., 2014).) These questions are addressed through a statistical analysis of MODIS (Moderate Resolution Imaging Spectroradiometer) observations, sometimes in conjunction with MERRA-2 (Modern-Era Retrospective analysis for Research and Applications, Version 2) global reanalysis data on aerosol properties. First, Section 2 examines the relationship between cloud fraction and aerosol optical depth, then Section 3 examines cloud-related variations in aerosol particle size. Finally, Section 4 provides a brief summary.

2 Relationship between cloud fraction and aerosol optical depth

Let us begin by analyzing the statistical relationship between CF and AOD (at 550 nm) using the MODIS Aqua Level 3 joint atmospheric product (Collection 6 version of MYD08 product files, see *Platnick et al.* [2015]). This product provides daily average values of aerosol and cloud properties on a 1° by 1° horizontal grid covering the whole globe. (At low to mid latitudes this daily average comes from a single observation in the early afternoon.) Our study uses daytime average values for June-July-August (JJA) and December-January-February (DJF) from 2012 to 2014. We note that our analysis does not use observations that indicate complete cloud cover or completely clear sky in an area, due the lack of aerosol or cloud data on such days. Also, in order to focus on aerosol-cloud interactions for low clouds, data values were used only when the MODIS-estimated mean cloud top height of a partly cloudy grid box [e.g., *Baum et al.*, 2012] was below 3 km. While this altitude limit eliminates the consideration of high clouds that are irrelevant to aerosols that occur mostly at lower altitudes, we note that some eliminated clouds that have high tops but low cloud base may have even greater influence on aerosols than the thinner, low-level clouds considered in this study.

Figure 2a shows that the correlation between daily daytime average CF and AOD values for June, July, and August (JJA) is positive over much of the globe, with the exception of some desert areas. Panel b then shows that over most areas, AOD is substantially higher—typically by 30-50%—on days when the cloud cover exceeds the local seasonal average than on days when cloud cover is below average. The results indicate that the global overall and regional relationships found in earlier studies truly extend over most of the globe (as opposed to coming either from a few dominating regions, or from some regions of the Earth being systematically both cloudier and more aerosol-laden than others). Also, the results are consistent with the results of *Loeb and Schuster* [2008], who found that cloud cover tended to be higher on more aerosol-laden days. We note that the results are similar for December, January, and February (DJF), though DJF data covers polar regions in the southern rather than northern hemisphere, due to seasonal changes in illumination and snow cover.

In order to examine how the CF-AOD relationship depends on aerosol type, we combine the MODIS data with aerosol type information from the MERRA-2 global reanalysis. The reanalysis data is provided by the GEOS-5 (Goddard Earth Observing System Model, Version 5)

global model that incorporates the GOCART (Goddard Chemistry, Aerosol, Radiation, and Transport) aerosol model [Chin *et al.*, 2002]. GOCART keeps track of five aerosol species: black and organic carbon, dust, sea salt, and sulfates. For simplicity, our analysis combines the black and organic carbon species into a single category. We note that while GOCART assimilates observations of aerosol amounts from MODIS, the distribution of various aerosol species comes from the model itself.

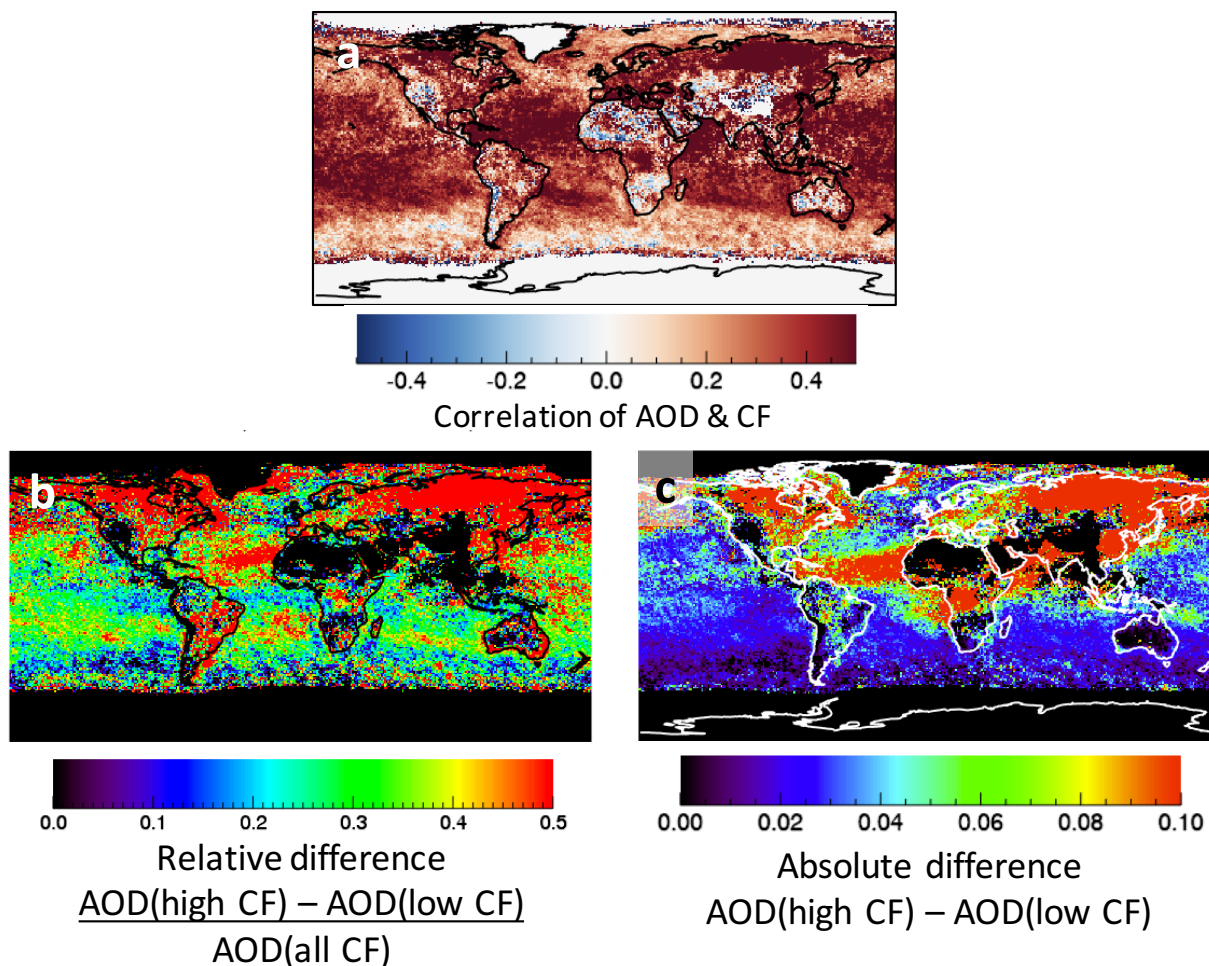


Figure 2. Geographical distribution of the relationship between cloud fraction and mean aerosol optical depth (at 550 nm) in JJA. (a) Map of CF-AOD correlation. (b) and (c) Maps of the relative and absolute differences between AOD values measured on days when cloud cover was higher or lower than the median cloud cover of each location.

Figure 3 shows the CF-AOD correlation derived from the MODIS data, but considering only those days when MERRA-2 indicated that a certain aerosol type dominated in the region (providing more than 50% of the total AOD in MERRA-2). Naturally, this means that observations from days with multiple evenly mixed aerosol types were not used. Moreover, the maps constructed separately for each aerosol type have large empty areas where the particular aerosol type never dominated. Overall, the results show a strong CF-AOD correlation for all aerosol types, even for the relatively less hygroscopic desert dust. This finding is consistent with the results in *Gryspeerd et al.* [2016], which indicate that the AOD of various aerosol species calculated in the MACC global reanalysis increases systematically with CF.

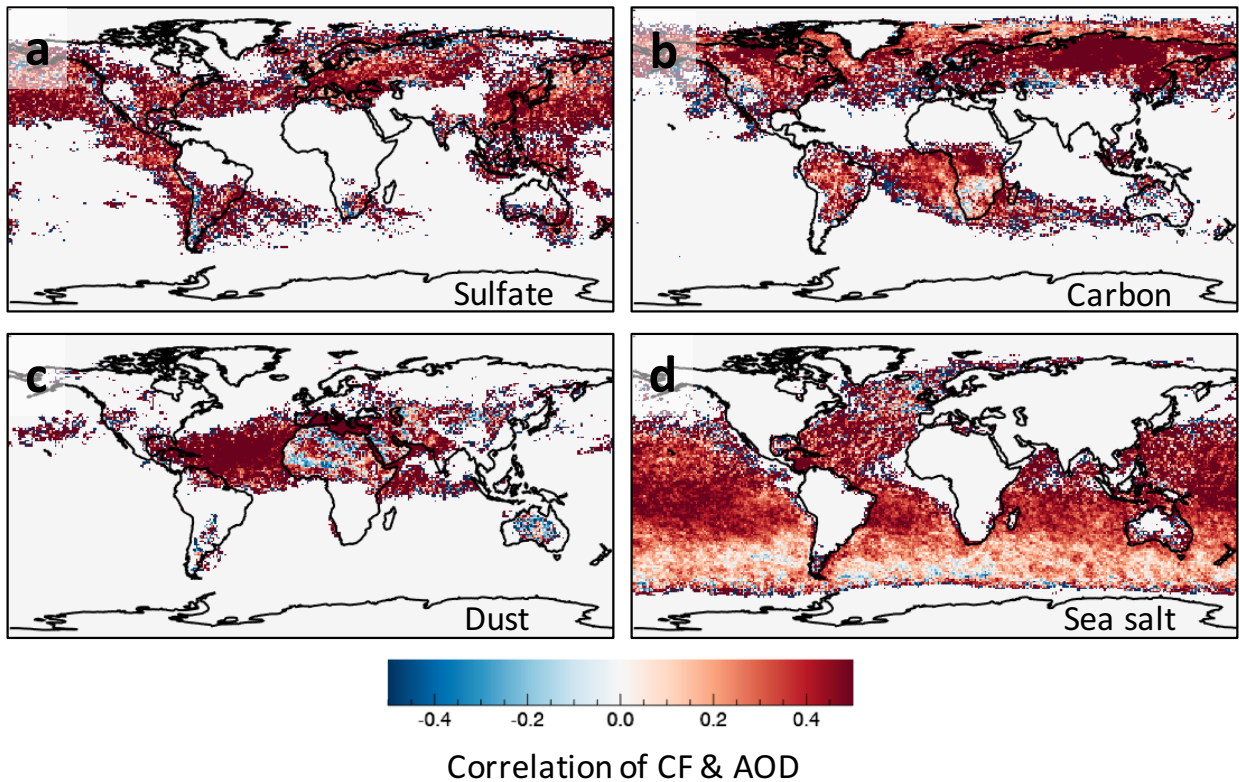


Figure 3. Maps of local CF-AOD correlation considering for each location only those days in JJA when the MERRA-2 reanalysis indicated that a single aerosol type dominated in 1° by 1° area. (a) Days dominated by sulfate aerosols (b) Days dominated by carbon aerosols (c) Days dominated by desert dust (d) Days dominated by sea salt. Zero values (white) indicate locations where there were not enough days dominated by a particular aerosol type to calculate CF-AOD correlations.

To summarize this section, all observations either on a pixel-by-pixel basis (Level 2 data-product, e.g., *Loeb and Manalo-Smith* [2005]; *Chand et al.* [2012]; and *Várnai and Marshak* [2014]) or averaged over space and time (Level 3 product) provide a clear signature of a positive correlation between CF and AOD. The combination of satellite data with the global reanalysis model MERRA-2 supports this correlation for all aerosol types considered.

3 Cloud-related changes in aerosol particle size

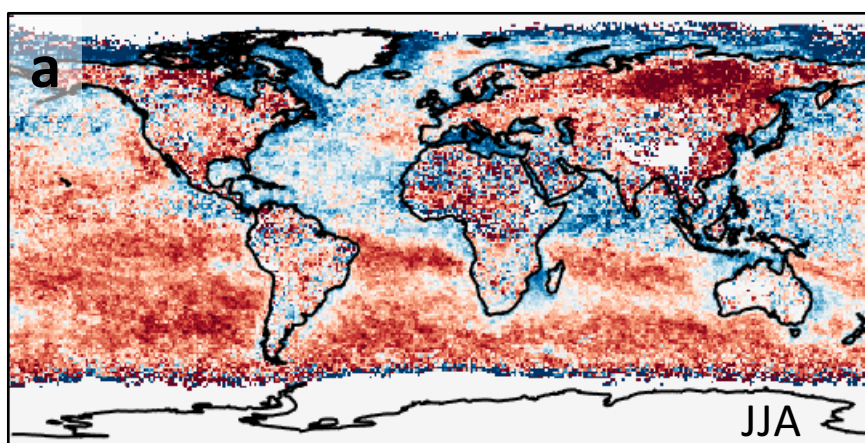
While all observations point to a similar statistical relationship between CF and AOD, this is not the case for the relationship between CF and particle size. To examine this relationship, Figure 4 shows global maps of the correlation between CF and aerosol Angstrom exponent (AE) in the MODIS Dark Target-Deep Blue combined product. In this product, AE data comes from the Deep Blue algorithm [*Hsu et al.*, 2004] over land (for 412-470 nm), and from the Dark Target algorithm [*Levy et al.*, 2013] over water (for 550-865 nm). Panel 4a reveals that in JJA, positive correlations dominate over much of the southern hemispheric oceans, but over northern hemispheric oceans there are large areas with both positive and negative correlations. Panel b shows that in DJF the two hemispheres are much more similar to each another, with positive but weaker correlations over most oceans. The figure also shows that large areas of both positive and negative correlations occur both over land and ocean. In other words, both the Dark Target and Deep Blue algorithms show that the effective aerosol particle size increases with cloudiness in some areas, and decreases in others.

We note that reflectances are more sensitive to the size of fine mode particles at shorter wavelengths than at longer ones. This means that for aerosol populations dominated by fine mode, AEs involving short wavelengths will depend on the exact wavelengths used (e.g., *Eck et al.*, 1999; *Reid et al.*, 1999). Therefore, the wavelength difference between AEs produced over land and ocean may explain the jumps in CF-AE correlations that occur at many coastlines, for example at the East coasts of Asia and North America in Fig. 4.

Let us mention that, in principle, the jump at coastlines can even help gain information on coastal aerosols if we assume that aerosol populations are similar on both sides of a coastline and

the accuracy of AE values [e.g., *Sayer et al.*, 2013] is sufficient. This is because the shorter wavelengths used for Angstrom exponents over land are sensitive to the fine mode effective radius, while the longer wavelengths used for Angstrom exponents over ocean are sensitive to the fine/coarse mode aerosol fractions [Schuster et al., 2006]. Thus, having positive CF-AE correlations on land (suggesting smaller fine mode particles for higher CF) and negative correlations over ocean (suggesting lower coarse mode fractions for higher CF) could be a sign of increasing cloudiness being linked to decreasing values of fine mode effective radii and coarse mode fractions in coastal areas.

We also note that while in Fig. 4, the correlations were calculated by giving all AE values equal weights, in some applications it is more appropriate to weigh AE values by the corresponding AOD. We found, however, that such weighting has little impact on the calculated correlations, and the maps based on AOD-weighted AE values (not shown) look almost identical to the maps in Fig. 4.



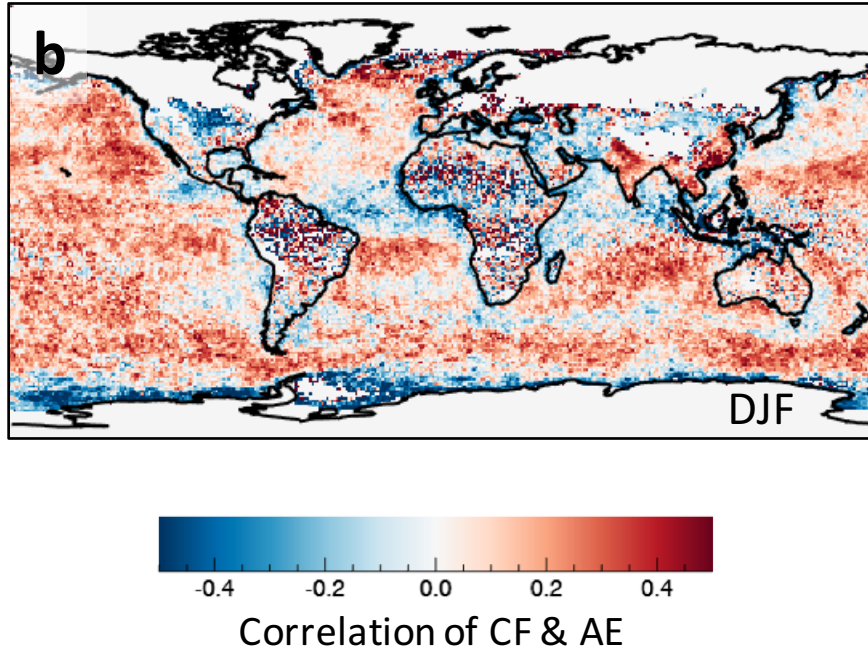


Figure 4. Map of the correlation between cloud fraction and Angstrom exponent in the MODIS dark target product over the ocean and the Deep Blue retrieval product over land.

Seeking further insights into the CF-AE correlations, let us examine the CF-AOD correlations separately for the coarse mode and fine mode AOD values provided in the Dark Target product [Kleidman *et al.*, 2005]. (The Deep Blue product does not provide separate AOD values for fine mode and coarse mode aerosols.) We note that in the MODIS Dark Target retrievals over ocean the assumed size of aerosol particles is fixed [Remer *et al.*, 2005], and so variations in AE correspond to variations in the relative amount of coarse mode and fine mode aerosols. In good agreement with the results in Fig. 3 of Eck *et al.* [2010], simple Mie calculations show that a hypothetical increase of 0.1 in AE corresponds to a decrease of about 0.05 in coarse mode fraction. This, in turn, implies a roughly 8% change in effective radius. To put this number in context, Mishchenko *et al.* [2004, 2007] argued that in order to reach an accuracy of 0.25 W/m^2 in aerosol radiative forcing estimations, the uncertainty in aerosol particle size measurements should be less than 10%.

A comparison of Figures 5a and 5b reveals that almost everywhere, CF is significantly more correlated with AOD for fine mode than for coarse mode aerosols. Figure 5c reveals that

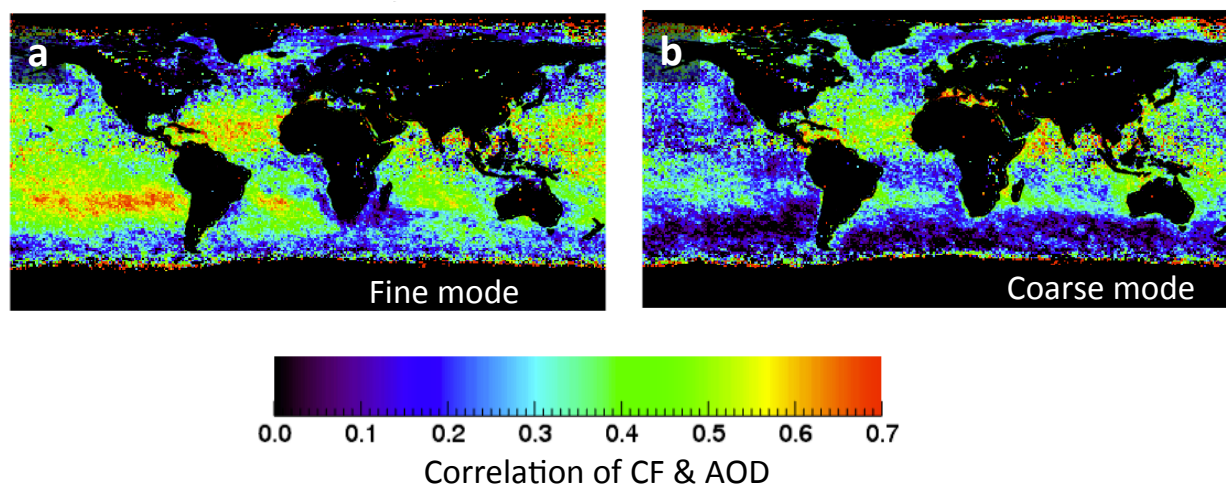
over much of the open oceans, the AOD difference between cloudier and less cloudy days is larger for fine mode than for coarse mode. The main exceptions are regions with substantial dust transport from deserts and some areas near land. (The opposite trend in these areas may be due, in part, to a misidentification of some pixels with thick dust as cloudy, which may increase the estimated cloud cover in heavy-dust regions.)

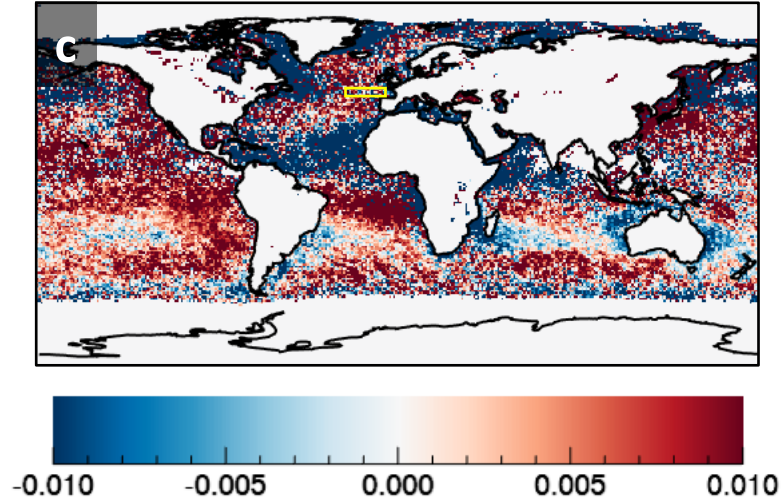
Let us point out that similar behaviors were also found in ground-based measurements [Eck *et al.*, 2014]. For example, the analysis of AERONET sun photometer observations during the DISCOVER-AQ campaign over Maryland found that as clouds developed during the day, AOD increases were dominated by fine mode rather than for coarse mode aerosols (e.g., Figures 5-7 in Eck *et al.* [2014]). The AERONET data also revealed that in some cases fine mode particle size increased with cloudiness as a result of humidification or cloud processing (their Fig. 6), while in other cases the fine mode shifted toward smaller sizes as a result of either new particle formation or humidification/cloud processing of very small particles (which made them large enough to become optically active) (their Fig. 7). We note that in all cases, the changes occurred at sizes much smaller than cloud droplets. This means that the basic findings cannot be attributed to cloud contamination, which should affect mostly coarse mode results.

Similarly to this conclusion for AERONET data, a key implication of our results in Fig. 5 is that over the large swaths of the oceans where AOD increases with CF more for fine mode than for coarse mode aerosols (i.e., red areas in Fig. 5c), cloud contamination is not the dominant reason for the CF-AOD correlations in MODIS data. We believe this based on the consideration that since undetected cloud drops are larger than most aerosols, they tend to have smaller AEs than bimodal aerosol populations. (The main exception would be areas where the fine mode is missing and coarse mode aerosols have slightly lower AEs than cloud droplets. However, this is not a typical case, as the average fine mode fraction is substantial in all oceanic regions [Remer *et al.*, 2008] and, as it will be shown later in this paper, the mean aerosol AE values over most oceans are much higher than the near-zero or even slightly negative values we can expect for cloud droplets.) Given their small AEs, undetected cloud drops tend to reduce the AEs of aerosol populations. Because aerosol retrievals interpret a drop in AE as a sign of an increase in coarse mode fraction (e.g., Eck *et al.* [2010]), undetected cloud droplets tend to increase the retrieved coarse mode fraction. Therefore when cloud contamination is the dominant cause of CF-AOD

correlations, AOD must increase with CF more for coarse mode than fine mode—which is not the case in the red-colored areas in Fig. 5c.

Naturally, this does not mean that cloud contamination does not occur (for example in partly cloudy pixels), or that its effect are not significant—only that in many areas it is not the dominant effect. The reason why it is not dominant is that data processing algorithms take extra care to minimize it. For example, the MODIS Dark Target algorithm shown in Figure 5 uses several steps to screen for clouds using various tests of brightness as well as spectral and spatial variability—and as an added precaution, it excludes the brightest 25% of pixels in an area even if they passed all tests [Martins *et al.*, 2002; Remer *et al.*, 2005].





$$(\text{AOD}_{\text{FM}}(\text{high CF}) - \text{AOD}_{\text{FM}}(\text{low CF})) - (\text{AOD}_{\text{CM}}(\text{high CF}) - \text{AOD}_{\text{CM}}(\text{low CF}))$$

Figure 5. Map of relationships between CF and AOD separately for fine and coarse mode aerosols. Panels a and b show CF-AOD correlations for (a) Fine mode; (b) Coarse mode. Panel c shows where the AOD difference between cloudier and less cloudy days is larger (or smaller) for fine mode than for coarse mode aerosols. The yellow rectangle in Panel c highlights the area used for the analysis in Figures 6 & 7. All data is for JJA.

While it is not yet certain why fine mode AOD varies more with CF than coarse mode AOD does, several factors may play a role, for example: (i) coarse mode aerosols—such as dust particles in the elevated Saharan Air Layer—may float well above boundary layer clouds and hence may not interact with them; (ii) fine mode aerosols are typically more hygroscopic and swell more in the humid air surrounding clouds; (iii) cloud processing or new particle formation may create small particles and/or more optically effective ones; (iv) sunlight scattered from clouds can bias satellite retrievals toward larger AOD values and smaller aerosol sizes through the 3D radiative process called bluing [Marshak *et al.*, 2008]. To help better understand aerosol-cloud interactions, future studies are needed to evaluate the relative importance of such factors.

One possibility for further analysis is to combine data from different sources. As a first step in this direction, we combine the MODIS Dark Target (DT) product with the MODIS Ocean Color product [Ahmad *et al.*, 2010]. Namely, we examine the impact of clouds on AE by combining 3 km-resolution MODIS Dark Target AE values with 1 km-resolution Quality

Assessment (QA) flags that warn about possible cloud impacts in the MODIS Ocean Color product. To allow comparisons with earlier results, the analysis is based on the same MODIS Aqua observations as in *Várnai and Marshak* [2009, 2015]: September 14-29 in the 2002-2011 period over the northeast Atlantic Ocean (45-50° N, 5-25°W). Let us point out, however, that based on Figs. 2, 4 and 5, this region appears to have relatively weak relationships between CF and AOD or AE. As a result, we expect that the tendencies discussed below are significantly stronger in many other regions of the Earth.

Following the approach of *Várnai and Marshak* [2015], Figures 6 and 7 of this study show results for pixels that are 3 and 6 km away from the nearest low-level clouds (cloud tops below 3km). CF values in Figures 6 and 7 are calculated as the cloud cover of low-level clouds in a 41 by 41 km surrounding area. The figures show results for four different subsets of all available data. The black lines are based on all data where the Dark Target QA flag indicates high quality retrievals ($DT\ QA \geq 1$). The blue lines are for those pixels with $DT\ QA \geq 1$ where the Ocean Color QA flag “straylight” warns about potential impacts from clouds that occur within the surrounding 5 by 7 km region from a bright cloudy pixel (<https://oceancolor.gsfc.nasa.gov/reprocessing/r2009/flags/>). The red lines are for those pixels with $DT\ QA \geq 1$ where the ocean color QA flag “sstwarn” warns about the possibility of cloud contamination. (This flag is based largely on the variability of 250 m-resolution 0.86 μm reflectances within 1 km-size areas and the variability of 1 km-resolution 11 μm brightness temperatures in 3 km-size areas. For details, see <https://oceancolor.gsfc.nasa.gov/atbd/sst/flag/>.) Finally, the green lines are for those pixels with $DT\ QA \geq 1$ where neither the straylight nor the sstwarn flags give warnings. (Note that the sum of green, red and blue lines in Panel a can exceed the black line because some pixels have warnings by both the straylight and sstwarn flags. We note that the uncertainties due to annual variability (estimated from the spread of results for individual years) are around 0.0035 for AOD and 0.03 for AE values.

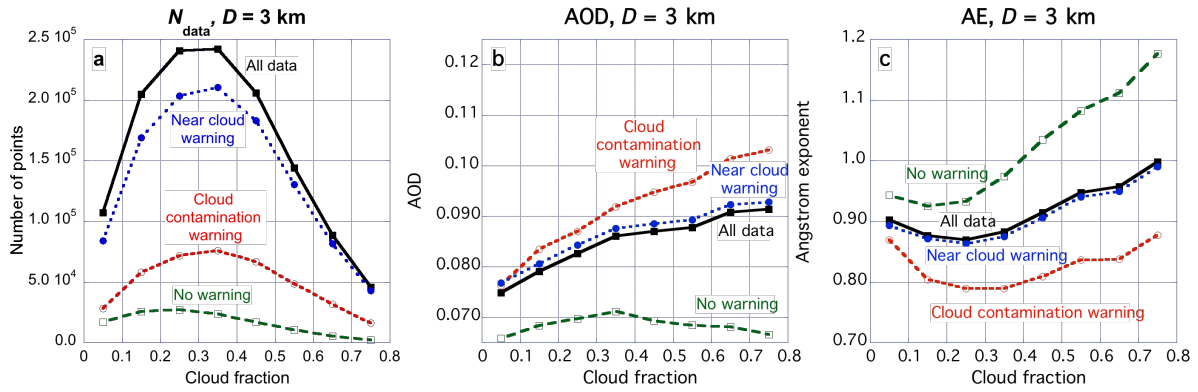


Figure 6. Impact of cloud-related Quality Assessment flags in the MODIS ocean color product on MODIS Dark Target aerosol data. (a) Number of pixels; (b) Aerosol Optical Depth (AOD); (c) Angstrom exponent. Figure is for September 14-29 in 2002-2011, for an area over the Northeast Atlantic Ocean (45-50°N, 5-25°W). Data is plotted for pixels that are 3 km away from the nearest low-level cloud.

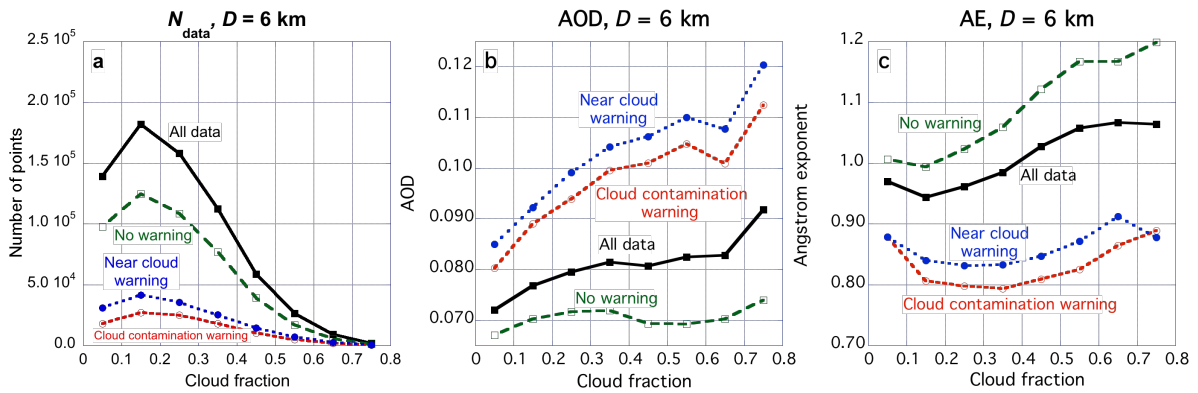


Figure 7. Same as Figure 6, but for pixels that are 6 km away from the nearest low-level cloud.

Figures 6a and 7a show that most pixels have cloud-related warnings 3 km away from clouds, but not 6 km away. (We note that most pixels with cloud contamination warning also have a near-cloud (that is, straylight) warning.) Figures 6b and 7b show that AOD does not change much with CF for pixels with no warnings about possible cloud effects, but it increases markedly for pixels with warnings. This suggests that the QA flags are largely successful in identifying cloud-affected areas (sometimes they might miss small thin clouds, or flag pixels that

are near not clouds but thick aerosol plumes). Figures 6c and 7c are more complicated to interpret. They show that fine mode aerosols dominated in the region, as all mean AE values are higher than the 0.75 value typically associated with 50% fine mode fraction of AOD at 500 nm [Eck *et al.*, 2010]. Figures 6c and 7c also show that the (443-869 nm) AE provided in the MODIS ocean color product increases (that is, effective particle size decreases) with CF for pixels with no warnings. As suggested in Várnai and Marshak [2015], this may occur because small pollution particles may dominate aerosol populations when cloudy weather systems bring air from North America or Europe, whereas large dust or sea salt particles may dominate on less cloudy days when the air is coming from deserts or subtropical oceanic areas. In contrast, the effective particle size in pixels with cloud-related warnings does not change significantly with CF, as the decrease with CF seen for pixels with no warnings is offset by an increase related to cloud-related processes such as humidification. Particle size is markedly larger (AE is smaller) for pixels with cloud-related warnings than for pixels without warnings (especially 3 km away from clouds, see Fig. 6c), and this size difference increases steadily with the amount of clouds. This allows us to conclude that cloud-impacted (near-cloud) pixels and possibly cloud-contaminated pixels tend to contain larger particles (plus cloud droplets) than other nearby pixels. Finally, let us point out that the results in Figs. 6 and 7 imply that aerosol particle number concentration increases with CF both for pixels with and without cloud-related warnings (increasing AOD with steady particle size and steady AOD with decreasing particle size, respectively).

Finally, Fig. 8 explores the relationship between the CF-AE correlation and AE itself. The map of mean AE values in Fig. 8a shows spatial patterns that are often the reverse of patterns for CF-AE correlations in Fig. 4a. This behavior is confirmed by Figure 8b, which shows that areas of small AE tend to have positive CF-AE correlations, whereas areas of large AE tend to have negative CF-AE correlations. This tendency can be explained by considering the hygroscopic swelling of fine mode particles, even if coarse mode particles remain unchanged. (For example, if coarse mode particles are less hygroscopic or float above the humid, partly cloudy boundary layer.) To demonstrate this, let us consider some simple Mie calculations for bimodal aerosol populations. The goal is to demonstrate that the same swelling of fine mode particles in broken cloud fields can have opposite effects on the overall AE, depending on the abundance of coarse mode particles. As an example, Figure 8c shows that if swelling increases

the median radius of fine mode particles from 0.07 to 0.12 μm , the overall (550-869 nm) AE of a bimodal particle population will decrease along the dashed blue line in cases of large AE (low coarse mode fraction), but will increase along the solid red line in cases of small AE (high coarse mode fraction). We note that the AE of the bimodal population increases along the red line even though the AE of fine particles actually decreases. Specifically, as the fine mode median radius increases from 0.07 to 0.12 μm and the coarse mode remains unchanged, the fine mode AE drops from 1.87 to 1.43 (not shown), the coarse mode AE remains constant at -0.13 (not shown), but the overall AE in Fig. 8c increases from 0.86 to 1.15. The overall AE increases because the swelling enhances the radiative impact of fine particles relative to the impact of coarse mode particles, and so the effective particle size of bimodal distributions shifts toward smaller sizes. (We note that even the blue curve would show an initial increase if swelling started at a smaller size: If fine particles started out so small that their light scattering was negligible, the overall AE would start out being the coarse mode AE. As fine particles then grew larger, the overall AE would increase to a value between the higher AE of fine-mode and lower AE of coarse mode.) The result that the same swelling (e.g., fine mode swelling from 0.07 to 0.12 μm) can cause opposite changes in AE depending on the fine/coarse mode fraction, illustrates that the sign of AE variations by itself cannot reveal the direction of particle size changes. Consequently, the effect of clouds on aerosol particle size cannot always be adequately described by changes in Angstrom exponent alone.

To summarize this section, the analysis of different MODIS aerosol products showed that over large regions of the Earth, effective aerosol particle size decreases with increasing cloudiness. This occurs because an increase in CF implies a larger AOD growth for fine mode than for coarse mode aerosols. The finding indicates that the observed correlations between CF and AOD do not come primarily from cloud detection uncertainties. Moreover, this section demonstrated a way in which cloud-related QA flags in the MODIS Ocean Color product can help identify MODIS aerosol data impacted by nearby clouds. Finally, the results revealed a duality in behaviors: Even when particle size does not increase with CF, it still increases in the proximity of clouds (e.g., Figs. 6 and 7 show larger particles at 3 km than at 6 km from clouds). This is possibly because variations in CF involve changes in the large-scale atmospheric environment (thus in aerosols), while the approach toward clouds occurs within the same large-

scale atmospheric environment and thus leads toward larger aerosol particles (as we see in both Ocean Color and Dark Target MODIS products).

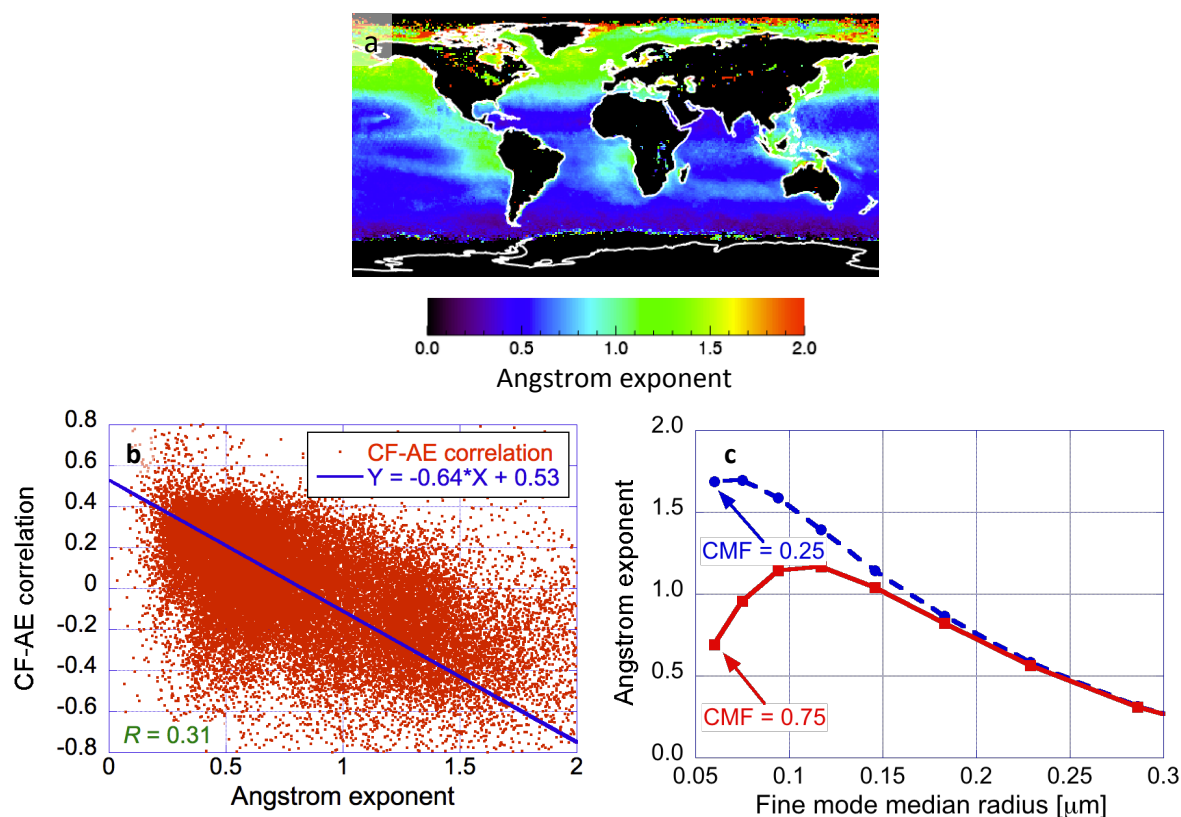


Figure 8. Relationship between CF-AE correlation and particle size. (a) Map of Dark Target mean AE values for JJA; (b) Comparison of individual values in the maps in Figures 4a and 8a. The position of each dot along the x-axis represents the mean AE value of a grid point in Fig 8a, while the position along the y-axis represents the CF-AE correlation of the same grid point in Fig. 4a. (c) Change in the overall AE of bimodal aerosol distributions when the size of fine mode particles increases through hygroscopic swelling. The plot shows results from Mie calculations assuming Models #2 and #9 of the MODIS Dark Target (ocean) algorithm for the fine and coarse modes, respectively (Levy et al., 2013). As Table 2 of Remer et al. (2005) shows, the median radii are 0.06 μm and 0.5 μm for the “unswollen” fine and coarse modes, respectively, while the standard deviations of lognormal size distributions are 0.6 μm and 0.8 μm , and the effective radii are 0.15 and 2.5 μm for the two modes, respectively. Hygroscopic swelling of fine mode

particles is simulated using the approach in Gassó et al. (2000). As fine particles swell from a median radius of 0.06 μm to 0.28 μm , their effective radius increases from 0.15 μm to 0.7 μm . The printed coarse mode fraction (CMF) values indicate what fraction of 550 nm optical thickness is due to coarse mode particles before any swelling. As fine mode particles swell, this fraction decreases.

4 Summary

The ultimate goal of this paper is to help better understand aerosol-cloud interactions—a leading cause of uncertainties in our estimates of human impacts on climate. To this end, it examines the statistical relationships between aerosol properties and the amount and distance of surrounding clouds in observations taken by the MODIS satellite instrument.

First, the paper sought a more detailed picture of the positive correlation between cloud fraction and aerosol optical depth reported in earlier studies. Analyzing a global dataset of daily mean aerosol and cloud properties over a 1° by 1° latitude-longitude grid during three summers and winters, the study found that the positive correlation in earlier global statistics is strong throughout the globe in both winter and summer (as opposed to coming from a few dominating regions or from systematic differences between clouds and aerosols in different regions or seasons). Over much of the globe, aerosol optical depth (AOD) was found to be 30-50% higher on days that were cloudier than average than on days that were less cloudy than average.

Combining MODIS observations with MERRA-2 global reanalysis data on aerosol type revealed that the correlation between cloud cover and AOD was strong for all considered aerosol types: sulfate, dust, carbon, and sea salt.

After the initial focus on AOD, the paper examined how aerosol size distribution (characterized through the Angstrom Exponent) changes in the presence of nearby clouds. We found strong regional variations in the size distribution shifts that occur near clouds. Some large regions displayed shifts toward larger aerosols near clouds that is intuitively consistent with aerosol growth in the humid air surrounding clouds or the presence of undetected cloud particles, and is also consistent with CALIOP results in Yang *et al.* [2014]. Other large regions, however, clearly showed shifts toward smaller aerosols near clouds in three different operational MODIS

aerosol products: the Dark Target and Deep Blue products in this study, and in the Ocean Color product in *Várnai and Marshak* [2015]. The results also indicated that the quality assessment flags in the Ocean Color product can help us compare aerosol properties provided in the Dark Target product at pixels likely affected and by clouds and at pixels likely not affected.

A more detailed look at the MODIS results revealed that when aerosol particle size distributions shift toward smaller particles in cloudier regions, this is due to a greater increase in the AOD of fine mode than coarse mode aerosols. The greater increase in fine mode AOD implies that the CF-AOD correlation discussed here and in earlier studies does not come predominantly from cloud contamination.

Additionally, the results revealed a duality in behaviors: Even when aerosol particle size does not increase with CF, it still increases in the proximity of clouds. This is because variations in CF involve changes in the large-scale atmospheric environment and thus in aerosols, while the approach toward clouds occurs within the same large-scale atmospheric environment and leads toward larger aerosol particles. This implies that aerosol behaviors in partly cloudy regions are not dominated by a single factor and instead involve several factors: some change (increase or decrease) particle size throughout the cloudy regions, while others increase particle size in the vicinity of individual clouds. Such factors include hygroscopic swelling, meteorological covariation of cloudiness and aerosols, 3D radiative interactions (bluing), undetected cloud droplets, new particle formation through liquid phase chemical processes, and cloud processing that merges aerosol particles via the collision-coalescence and eventual evaporation of cloud droplets forming around them. The importance of each of these factors need to be evaluated in future studies.

The results also revealed that the hygroscopic swelling of fine mode particles can either decrease or increase the overall Angstrom exponent of bimodal particle populations. The swelling of fine mode particles always decreases their own Angstrom exponent, but at the same time it can enhance the radiative impact of fine mode particles relative to coarse mode particles, if coarse mode aerosols are less hygroscopic or float above the humid, partly cloudy boundary layer. The greater relative importance of the fine mode can in turn lead to an increase in overall Angstrom exponent. This implies that the sign of Angstrom exponent variations does not

necessarily indicate the direction of particle size changes, and that the effect of clouds on aerosol particle size cannot always be adequately described by changes in Angstrom exponent alone.

Although the methodology of data processing is also likely to impact the magnitude or in some cases even the sign of near-cloud particle size changes [e.g., *Ignatov et al.*, 2005], the finding of similar behaviors in three operational data products that use very different cloud detection, data selection, and aerosol retrieval algorithms suggests that the observed behaviors are not caused by data processing issues. We note, however, that CALIOP does not seem to show the diversity of behaviors observed by MODIS, and further study is needed to determine whether differences in cloud detection or data sampling may contribute to CALIOP consistently reporting larger particles near clouds [e.g., *Yang et al.*, 2014].

Acknowledgments

We gratefully acknowledge support for this research by the NASA Radiation Sciences Program managed by Hal Maring. We are grateful to Stephanie Huang for providing insights into near-cloud trends in Aeronet observations. We also thank Alexander Ignatov, Johannes Quaas, and Weidong Yang for insightful discussions and help. The MODIS data used in this study was obtained from the NASA Level-1 and Atmosphere Archive & Distribution System (<https://ladsweb.modaps.eosdis.nasa.gov>).

References

- Ahmad, Z., B. A. Franz, C. R. McClain, E. J. Kwiatkowska, J. Werdell, E. P. Shettle, and B. N. Holben (2010), New aerosol models for the retrieval of aerosol optical thickness and normalized water-leaving radiances from the SeaWiFS and MODIS sensors over coastal regions and open oceans, *Appl. Opt.*, 49, 5545–5560.
- Albrecht, B. A. (1981), Parameterization of trade-cumulus cloud amount, *J. Atmos. Sci.*, 38, 97–105.

- Baum, B., W. Menzel, R. Frey, D. Tobin, R. Holz, S. Ackerman, A. Heidinger, and P. Yang (2012), MODIS Cloud-Top Property Refinements for Collection 6. *J. Appl. Meteor. Climatol.*, 51, 1145–1163, doi: 10.1175/JAMC-D-11-0203.1.
- Chand, D., R. Wood, S. Ghan, M. Wang, M. Ovchinnikov, P. J. Rasch, S. Miller, B. Schichtel, T. Moore (2012), Aerosol optical depth enhancement in partly cloudy conditions. *J. Geophys. Res.*, 117, D17207, doi:10.1029/2012JD017894.
- Chen, Y-C., M. W. Christensen, G. L. Stephens, and J. H. Seinfeld (2014), Satellite-based estimate of global aerosol–cloud radiative forcing by marine warm clouds. *Nature Geoscience*, 7, 643–646.
- Chin, M., P. Ginoux, S. Kinne, B. N. Holben, B. N. Duncan, R. V. Martin, J. A. Logan, A. Higurashi, and T. Nakajima (2002), Tropospheric aerosol optical thickness from the GOCART model and comparisons with satellite and sunphotometer measurements, *J. Atmos. Sci.* 59, 461–483.
- Eck, T. F., B. N. Holben, J. S. Reid, O. Dubovik, A. Smirnov, N. T. O'Neill, I. Slutsker, and S. Kinne (1999), Wavelength dependence of the optical depth of biomass burning, urban and desert dust aerosols, *J. Geophys. Res.*, 104, 31 333–31 350.
- Eck, T. F., B. N. Holben, A. Sinyuk, R. T. Pinker, P. Goloub, H. Chen, B. Chatenet, Z. Li, R. P. Singh, S. N. Tripathi, J. S. Reid, D. M. Giles, O. Dubovik, N. T. O'Neill, A. Smirnov, P. Wang, X. Xia (2010), Climatological aspects of the optical properties of fine/coarse mode aerosol mixtures, *J. Geophys. Res.*, 115, D19205, doi: 10.1029/2010JD014002.
- Eck, T. F., B. N. Holben, J. S. Reid, D. M. Giles, M. A. Rivas, R. P. Singh, S. N. Tripathi, C. J. Bruegge, S. Platnick, G. T. Arnold, N. A. Krotkov, S. A. Carn, A. Sinyuk, O. Dubovik, A. Arola, J. S. Schafer, P. Artaxo, A. Smirnov, H. Chen, and P. Goloub (2012), Fog- and cloud-induced aerosol modification observed by the Aerosol Robotic Network (AERONET), *J. Geophys. Res.*, 117, D07206, doi:10.1029/2011JD016839.
- Eck, T. F., B. N. Holben, J. S. Reid, A. Arola, R. A. Ferrare, C. A. Hostetler, S. N. Crumeyrolle, T. A. Berkoff, E. J. Welton, S. Lolli, A. Lyapustin, Y. Wang, J. S. Schafer, D. M. Giles, B. E.

503 Anderson, K. L. Thornhill, P. Minnis, K. E. Pickering, C. P. Loughner, A. Smirnov, and A.
 504 Sinyuk, (2014), Observations of rapid aerosol optical depth enhancements in the vicinity of
 505 polluted cumulus clouds, *Atmos. Chem. Phys.*, 14, 11633-11656, doi:10.5194/acp-14-11633-
 506 2014.

507 Ervens, B.; B. J. Turpin, R. J. Weber (2011), Secondary organic aerosol formation in cloud
 508 droplets and aqueous particles (aqSOA): A review of laboratory, field and model studies, *Atmos.*
 509 *Chem. Phys.* 2011, 11, 11069–11102.

510 Grandey, B. S., Stier, P., and Wagner, T. M.: Investigating relationships between aerosol optical
 511 depth and cloud fraction using satellite, aerosol reanalysis and general circulation model data,
 512 *Atmos. Chem. Phys.*, 13, 3177-3184, <https://doi.org/10.5194/acp-13-3177-2013>, 2013.

513 Gryspeerdt, E., J. Quaas, and N. Bellouin (2016), Constraining the aerosol influence on cloud
 514 fraction, *J. Geophys. Res.*, 121, 3566–3583, doi:10.1002/2015JD023744.

515 Hsu, N. C., S.-C. Tsay, M. D. King, and J. R. Herman (2004), Aerosol properties over bright-
 516 reflecting source regions, *IEEE Trans. Geosci. Remote Sens.*, 42(3), 557–569,
 517 doi:10.1109/TGRS.2004.824067.

518 Ignatov A., P. Minnis, N.G. Loeb, B. Wielicki, W. Miller, S. Sun-Mack, D. Tanre, L.A. Remer,
 519 I. Laszlo, E. Geier (2005), Two MODIS aerosol products over ocean on the Terra and Aqua
 520 CERES SSF, *J. Atmos. Sci.*, 62, 1008-1031.

521 IPCC AR5 (2013), Climate Change 2013: The Physical Science Basis. Contribution of Working
 522 Group I to the Fifth Assessment Report of the Intergovern- mental Panel on Climate Change
 523 [Stocker, T.F., D. Qin, G.-K. Plattner, M. Tignor, S.K. Allen, J. Boschung, A. Nauels, Y. Xia, V.
 524 Bex and P.M. Midgley (eds.)]. Cambridge University Press, Cambridge, United Kingdom and
 525 New York, NY, USA, 1535 pp.

526 Jeong, M. J., and Z. Li (2010), Separating real and apparent effects of cloud, humidity, and
 527 dynamics on aerosol optical thickness near cloud edges. *J. Geophys. Res.*, 115, D00K32.

Kaufman, Y., Koren, I., Remer, L., Rosenfeld, D., Rudich, Y. 2005. The Effect of Smoke Dust and Pollution Aerosol on Shallow Cloud Development Over the Atlantic Ocean. *Proceedings of the National Academy of Sciences*, 102, 11207-11212. doi: 10.1073/pnas.0505191102.

Kerkweg, A.; S. Wurzler, T. Reisin, A. Bott (2003), On the cloud processing of aerosol particles: An entraining air-parcel model with two-dimensional spectral cloud microphysics and a new formulation of the collection kernel, *Q. J. Roy. Meteorol. Soc.*, 129, 1–18.

Kleidman, R. G., N. T. O'Neill, L. A. Remer, Y. J. Kaufman, T. F. Eck, D. Tanré, O. Dubovik, and B. N. Holben (2005), Comparison of Moderate Resolution Imaging Spectroradiometer (MODIS) and Aerosol Robotic Network (AERONET) remote-sensing retrievals of aerosol fine mode fraction over ocean, *J. Geophys. Res.*, 110, D22205, doi:10.1029/2005JD005760.

Koren, I., L. A. Remer, Y. J. Kaufman, Y. Rudich, and J. V. Martins (2007), On the twilight zone between clouds and aerosols. *Geophys. Res. Lett.*, 34, L08805, doi:10.1029/2007GL029253.

Koren, I., G. Feingold, H. Jiang, and O. Altaratz (2009), Aerosol effects on the inter-cloud region of a small cumulus cloud field, *Geophys. Res. Lett.*, 36, L14805, doi:10.1029/2009GL037424.

Levy, R. C., Mattoo, S., Munchak, L. A., Remer, L. A., Sayer, A. M., Patadia, F., and N. C. Hsu (2013), The Collection 6 MODIS aerosol products over land and ocean. *Atmos. Meas. Tech.*, 6, 2989–3034. doi:10.5194/amt-6-2989-2013

Loeb, N. G., and N. Manalo-Smith (2005), Top-of-Atmosphere direct radiative effect of aerosols over global oceans from merged CERES and MODIS observations. *J. Climate*, 18, 3506–3526. doi: 10.1175/JCLI3504.1.

Loeb, N. G., and G. L. Schuster (2008), An observational study of the relationship between cloud, aerosol and meteorology in broken low-level cloud conditions. *J. Geophys. Res.*, 113, D14214, doi:10.1029/2007JD009763.

Marshak A., G. Wen, J. Coakley, L. A. Remer, N. G. Loeb, R. F. Cahalan (2008), A simple model for the cloud adjacency effect and the apparent bluing of aerosols near clouds. *J. Geophys. Res.*, 113, D14S17.

555 Martins, J. V., D. Tanré, L. A. Remer, Y. J. Kaufman, S. Mattoo, and R. Levy (2002), MODIS
 556 cloud screening for remote sensing of aerosol over oceans using spatial variability. *Geophys.*
 557 *Res. Lett.*, 29, 8009, doi:10.1029/2001GL013252.

558 Mishchenko, M.I., B. Cairns, J.E. Hansen, L.D. Travis, R. Burg, Y.J. Kaufman, J.V. Martins, and
 559 E.P. Shettle (2004), Monitoring of aerosol forcing of climate from space: Analysis of
 560 measurement requirements. *J. Quant. Spectrosc. Radiat. Transfer*, 88, 149-161,
 561 doi:10.1016/j.jqsrt.2004.03.030.

562 Mishchenko, M.I., B. Cairns, G. Kopp, C.F. Schueler, B.A. Fafaul, J.E. Hansen, R.J. Hooker, T.
 563 Itchkawich, H.B. Maring, and L.D. Travis (2007), Accurate monitoring of terrestrial aerosols and
 564 total solar irradiance: Introducing the Glory mission, *Bull. Amer. Meteorol. Soc.*, 88, 677-691,
 565 doi:10.1175/BAMS-88-5-677.

566 Platnick, S., et al., (2015), MODIS Atmosphere L2 Joint Atmosphere Product. NASA MODIS
 567 Adaptive Processing System, Goddard Space Flight Center, USA:
 568 <http://dx.doi.org/10.5067/MODIS/MYDATML2.006>

569 Quaas, J., B. Stevens, P. Stier, and U. Lohmann (2010), Interpreting the cloud cover – aerosol
 570 optical depth relationship found in satellite data using a general circulation model. *Atmos. Chem.*
 571 *Phys.*, 10, 6129–6135, doi:10.5194/acp-10-6129-2010.

572 Reid, J. S., T. F. Eck, S. A. Christopher, P. V. Hobbs, and B. Holben (1999), Use of the
 573 Ångström exponent to estimate the variability of optical and physical properties of aging smoke
 574 particles in Brazil, *J. Geophys. Res.*, 104(D22), 27473–27489, doi:10.1029/1999JD900833.

575 Remer, L. A., Y. J. Kaufman, D. Tanre, S. Mattoo, D. A. Chu, J. V. Martins, R. R. Li, C. Ichoku,
 576 R. C. Levy, R. G. Kleidman, T. F. Eck, E. Vermote, and B. N. Holben (2005), The MODIS
 577 aerosol algorithm, products and validation. *J. Atmos. Sci.*, 62, 947-973.

578 Remer, L. A., R. G. Kleidman, R. C. Levy, Y. J. Kaufman, D. Tanré, S. Mattoo, J. V. Martins,
 579 C. Ichoku, I. Koren, H. Yu, and B. N. Holben (2008), Global aerosol climatology from the
 580 MODIS satellite sensors. *J. Geophys. Res.*, 113, D14S07, doi:10.1029/2007JD009661.

581 Sayer, A. M., N. C. Hsu, C. Bettenhausen, and M.-J. Jeong (2013), Validation and uncertainty
582 estimates for MODIS Collection 6 “Deep Blue” aerosol data, *J. Geophys. Res.*, 118, 7864–7872,
583 doi:10.1002/jgrd.50600.

584 Schuster, G. L., O. Dubovik, and B. N. Holben (2006), Angstrom exponent and bimodal aerosol
585 size distributions, *J. Geophys. Res.*, 111, D07207, doi:10.1029/2005JD006328.

586 Su, W., G. L. Schuster, N. G. Loeb, R. R. Rogers, R. A. Ferrare, C. A. Hostetler, J. W. Hair, and
587 M. D. Obland (2008), Aerosol and cloud interaction observed from high spectral resolution lidar
588 data. *J. Geophys. Res.*, 113, D24202, doi:10.1029/2008JD010588.

589 Tackett, J.L. and L. Di Girolamo (2009), Enhanced aerosol backscatter adjacent to tropical trade
590 wind clouds revealed by satellite-based lidar. *Geophys. Res. Lett.*, 36, L14804, doi:
591 10.1029/2009GL039264.

592 Ten Hoeve, J. E., and J. A. Augustine (2016), Aerosol effects on cloud cover as evidenced by
593 ground-based and space- based observations at five rural sites in the United States, *Geophys.*
594 *Res. Lett.*, 43, 793–801, doi:10.1002/2015GL066873.

595 Twohy, C. H., J. A. Coakley Jr., W.R. Tahnk (2009), Effect of changes in relative humidity on
596 aerosol scattering near clouds. *J. Geophys. Res.*, 114, D05205.

597 Várnai, T., and A. Marshak (2009), MODIS observations of enhanced clear sky reflectance near
598 clouds. *Geophys. Res. Lett.*, 36, L06807, doi:10.1029/2008GL037089.

599 Várnai, T., and A. Marshak (2014), Near-cloud aerosol properties from the 1-km resolution
600 MODIS ocean product. *J. Geophys. Res.*, 119, doi:10.1002/2013JD020633.

601 Várnai, T., and A. Marshak (2015), Effect of cloud fraction on near-cloud aerosol behavior in the
602 MODIS atmospheric correction ocean color product. *Remote Sens.*, 7, 5283-5299;
603 doi:10.3390/rs70505283.

604 Várnai, T., A. Marshak, and W. Yang (2013), Multi-satellite aerosol observations in the vicinity
605 of clouds. *Atmos. Chem. Phys.*, 13, 3899-3908, doi:10.5194/acp-13-3899- 2013.

606 Wen G., A. Marshak, and R. F. Cahalan (2008), Importance of molecular Rayleigh scattering in
607 the enhancement of clear sky radiance in the vicinity of boundary layer cumulus clouds. *J.*
608 *Geophys. Res.*, 113, D24207, doi:10.1029/2008JD010592.

609 Yang, W, A. Marshak, T. Várnai and R. Wood (2014), CALIPSO observations of near- cloud
610 aerosol properties as a function of cloud fraction. *Geoph. Res. Lett.*, 41, doi:
611 10.1002/2014GL061896.

612 Zhang, J., J. S. Reid, and B. N. Holben (2005), An analysis of potential cloud artifacts in MODIS
613 over ocean aerosol optical thickness products. *Geophys. Res. Lett.*, 32, L15803,
614 doi:10.1029/2005GL023254.

615